

Heat Transfer Engineering



Date: 05 July 2017, At: 08:03

ISSN: 0145-7632 (Print) 1521-0537 (Online) Journal homepage: http://www.tandfonline.com/loi/uhte20

Natural-Convection Heat Transfer in Channels With Isoflux Convex Surfaces

Fadl Moukalled & Issam Lakkis

To cite this article: Fadl Moukalled & Issam Lakkis (2009) Natural-Convection Heat Transfer in Channels With Isoflux Convex Surfaces, Heat Transfer Engineering, 30:14, 1151-1165, DOI: 10.1080/01457630902972751

To link to this article: http://dx.doi.org/10.1080/01457630902972751

	Published online: 10 Oct 2011.
Ø.	Submit your article to this journal 🗷
ılıl	Article views: 115
Q ^N	View related articles 🗷
4	Citing articles: 2 View citing articles 🗗

Full Terms & Conditions of access and use can be found at http://www.tandfonline.com/action/journalInformation?journalCode=uhte20

Heat Transfer Engineering, 30(14):1151-1165, 2009 Copyright © Taylor and Francis Group, LLC ISSN: 0145-7632 print / 1521-0537 online DOI: 10.1080/01457630902972751

Taylor & Francis
Taylor & Francis Group

Natural-Convection Heat Transfer in Channels With Isoflux Convex Surfaces

FADL MOUKALLED and ISSAM LAKKIS

Department of Mechanical Engineering, American University of Beirut, Beirut, Lebanon

Numerical solutions are presented for laminar natural convection heat transfer in channels with convex surfaces that are subjected to a uniform heat flux. Simulations are conducted for several values of Grashof number ($10 \text{ to } 10^4$) and radius of curvature ($1 \text{ to } \infty$). The governing elliptic conservation equations are solved in a boundary-fitted coordinate system using a collocated control-volume-based numerical procedure. The results are presented in terms of streamline and isotherm plots, inlet mass flow rates, curved wall temperature profiles, maximum hot wall temperature estimates, and average Nusselt number values. At the lowest radius of curvature, computations reveal the formation of recirculation zones in the exit section for all values of Grashof number considered. For a radius of curvature equal to or greater than 2, recirculation does not occur at any Grashof number. For values of radius of curvature between 1 and 2, the value of Grashof number at which recirculation occurs decreases with increasing values of the former. The variation in the buoyancy-induced volume flow rate is highly nonlinear with respect to the radius of curvature, and the value of the radius of curvature at which the volume flow rate is maximum increases with increasing Grashof number. The value of radius of curvature at which the maximum hot wall temperature is minimized increases with Grashof number. For all configurations studied, the average Nusselt number increases with increasing Grashof number values. Correlations for maximum wall temperature and average Nusselt number are provided.

INTRODUCTION

A large variety of industrial uses involve natural convection flow in pipes and rectangular channels. In some of these applications, heat transfer in conduits bounded by curved planes is of interest (e.g., flow in chimneys and fume hoods). In other applications, such as energy conservation in buildings, studies aimed at determining the shape that optimizes natural convection heat transfer are yet to be performed. The present investigation is geared toward such applications and focuses on natural convection heat transfer in channels having curved walls (see Figure 1a). The configuration of interest arises in systems involving an array of heat-generating devices that are submerged in liquid to enhance cooling (Figure 1b) and are enclosed by shells. The outer walls of any two consecutive shells form a channel with

The computational resources provided by the Center for Advanced Mathematical Sciences (CAMS) at the American University of Beirut (AUB) through the "Ibnsina" cluster are gratefully acknowledged.

Address correspondence to Professor Fadl Moukalled, Department of Mechanical Engineering, American University of Beirut, PO Box 11-0236, Riad El Solh, Beirut 1107 2020, Lebanon. E-mail: memouk@aub.edu.lb

convex walls. The vertical adiabatic extensions shown in Figure 1b are used to guide the flow and/or to prevent the hot fluid from flowing over other sensitive devices. A goal of this work is to evaluate the effect of wall curvature on the flow and the natural convection heat transfer, which are expected to be more complex than their counterparts in straight vertical channels and pipes. The complexity arises from the competing effects caused by the increase in the flow cross-sectional area (channel expansion) and the heat transfer area (length of curved wall) as compared to natural convection in a straight vertical channel of equal height. The increase in the heat transfer area intensifies the natural convection heat transfer, while an increase in the flow cross-sectional area increases the adverse pressure gradient that opposes the buoyancy-induced acceleration.

Many researchers have investigated [1–6] natural convection heat transfer in straight vertical channels with several types of boundary conditions imposed at the channel walls. Elenbaas [1] and Bodoia and Osterle [2] studied experimentally and numerically, respectively, the natural convection heat transfer in straight vertical channels with isothermal walls. Aung et al. [3] reported results in a channel with a prescribed heat flux

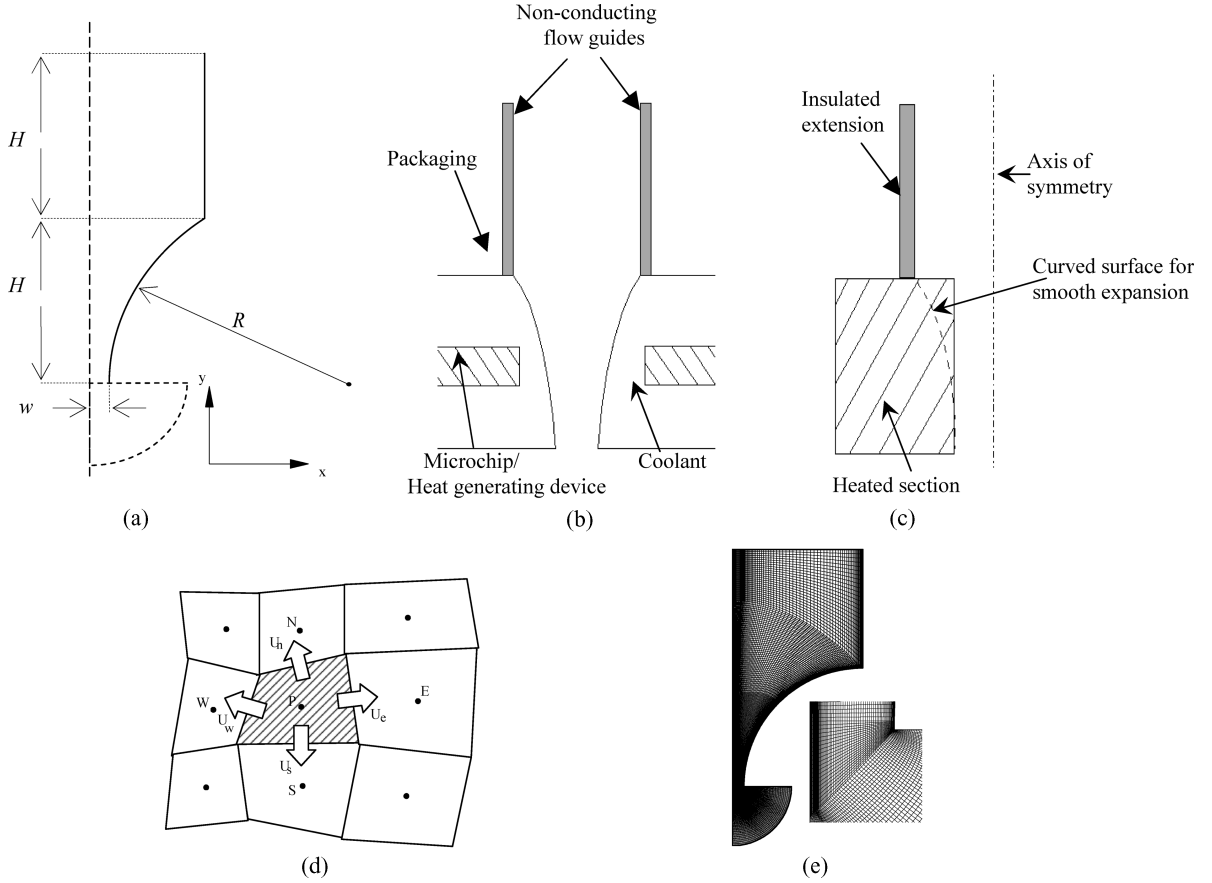


Figure 1 (a) Computational domain, (b) physical domain, (c) configuration studied by Manca et al. [19], (d) a typical control volume, and (e) grid network for $\kappa = 1$.

boundary condition at the walls, while Sparrow et al. [4] and Nieckle and Azevedo [5] analyzed the natural convection flow in straight vertical channels with one isothermal wall and one insulated wall. Haaland and Sparrow [6] presented a numerical solution for natural convection in a vertical channel with a point source and a distributed heat source placed at the inlet section.

Several studies dealing with natural convection in converging and diverging channels were also reported [7–13]. Work in converging channels includes the experimental investigation conducted by Kihm et al. [7] and the numerical investigations reported by Said [8] and Kaiser et al. [9]. Research in converging and in diverging channels includes the numerical computations performed by Marcondes et al. [10] and Langellotto et al. [11], and the experimental and numerical results generated by Sparrow and Ruiz [12] and Shalash et al. [13].

To increase the buoyancy-induced mass flow rates and heat transfer coefficients, unheated extensions were added to channels. Such configurations have been denoted in the literature by the channel-chimney systems. Several researchers [14–20] reported on the "chimney effect" in straight vertical channels. Straatman et al. [14] conducted a numerical and experimental investigation of free convection heat transfer in vertical channels with isothermal walls. Their results indicated an enhancement in heat transfer with adiabatic extensions. A correlation of average

Nusselt number in terms of the channel Rayleigh number, expansion ratio, and extension ratio was proposed. Auletta et al. [15] and Manca et al. [16] studied experimentally the effect of adding adiabatic extensions downstream from a vertical channel heated with a constant heat flux either symmetrically [15] or asymmetrically [16]. Results presented in [15] revealed that optimal enhancement in heat transfer is obtained with insulated extensions that are about three times the channel height and with an expansion ratio of around 2 for all configurations. Results documented in [16] indicate better system performance with a larger chimney. Lee [17] investigated numerically the effects of the unheated entry and unheated exit sections on natural convection heat transfer in vertical parallel plate channels symmetrically heated at either a uniform temperature or a uniform heat flux. Results reflected larger heat transfer and higher volume flow rate in an unheated exit section. Manca et al. [18, 19] performed experiments for natural convection of air in symmetrically and asymmetrically heated vertical channels with an adiabatic extension and showed that for the largest aspect ratio the adiabatic extensions lower the maximum wall temperature of the channel. An experimental study exploring the effect of the channel expansion and extension ratios on the buoyancy driven flow in symmetrically heated vertical channel-chimney systems was carried out by Auletta and Manca [20]. Campo et al. [21]

investigated the effect on natural convection heat transfer of appending insulated extensions at either the inlet or the exit to a parallel-plate channel in which the walls are heated at a uniform heat flux. Andreozzi et al. [22] conducted a numerical study of natural convection heat transfer in a channel–chimney system heated symmetrically at uniform heat flux. Andreozzi et al. [23] analyzed the combined effects on natural convection heat transfer of placing an unheated auxiliary plate at the inlet to and appending insulated extensions at the exit from a parallel-plate channel symmetrically heated at a uniform heat flux.

Pop and Takhar [24] and Magyari et al. [25] analyzed the free convective flow over a heated two-dimensional curved surface. Nakayama et al. [26] and Char and Chang [27] considered the same problem for the situation where the heated curved surface was embedded in a fluid-saturated porous medium and in a micropolar fluid, respectively. These studies demonstrated the existence of curved surfaces with temperature distributions, which permit similarity solutions of the power-law type. The equation of the corresponding shape curves was expressed either in terms of a series expansion [24, 25] or in terms of Gauss's hypergeometric function [25].

The configuration selected for the current investigation (Figure 1a) is the one that was used by Moukalled et al. [28, 29] and Lakkis and Moukalled [30] in their respective numerical studies of mixed convection and natural convection heat transfer in a channel with an isothermally heated convex surface bounded by a vertical adiabatic extension. The same configuration could also be seen as a variation of the work reported by Manca et al. [19], whereby to increase heat transfer a sudden expansion of the channel was suggested (Figure 1c). In this work a smooth expansion is proposed.

The intent of this article is to extend the work reported in [30] into situations where the convex surface is heated with a uniform flux.

PHYSICAL MODEL AND GOVERNING EQUATIONS

A schematic of the physical domain under consideration is depicted in Figure 1a. Because of symmetry, computations are performed only on the right half of the channel. The curved wall constitutes part of a circle with a radius of R and is heated with a uniform flux of strength \dot{q}_w ; the upper vertical wall is insulated. The difference between the surrounding fluid temperature, T_{∞} , and the convex surface temperature, $T_w(x, y)$, creates density variations within the fluid and gives rise to the buoyancy forces that move the flow into the channel through the bottom.

Upon defining the following dimensionless variables,

$$x = \frac{X}{w}, \ y = \frac{Y}{w}, \ \kappa = \frac{R/w}{H/w}, \ u = \frac{\rho U w}{\mu G r^{1/2}}, \ v = \frac{\rho V w}{\mu G r^{1/2}},$$

$$p = \frac{\rho P w^2}{\mu^2 G r^{1/2}}, \ \theta = \frac{T - T_{\infty}}{\dot{q}_w w/k}$$
 (1)

heat transfer engineering

and employing the Boussinesq approximation, with the thermophysical properties of the working fluid (considered to be air) assumed to be constant, except for density variations in the body force term, the equations, in dimensionless form governing conservation of mass, momentum, and energy, are respectively written as:

$$\frac{\partial u}{\partial x} + \frac{\partial v}{\partial y} = 0 \tag{2}$$

$$Gr^{1/2}\left(u\frac{\partial u}{\partial x} + v\frac{\partial u}{\partial y}\right) = \frac{\partial^2 u}{\partial x^2} + \frac{\partial^2 u}{\partial y^2} - \frac{\partial p}{\partial x}$$
(3)

$$Gr^{1/2}\left(u\frac{\partial v}{\partial x} + v\frac{\partial v}{\partial y}\right) = \frac{\partial^2 v}{\partial x^2} + \frac{\partial^2 v}{\partial y^2} - \frac{\partial p}{\partial y} + Gr^{1/2}\theta \quad (4)$$

$$Gr^{1/2}\left(u\frac{\partial\theta}{\partial x} + v\frac{\partial\theta}{\partial y}\right) = \frac{1}{\Pr}\left(\frac{\partial^2\theta}{\partial x^2} + \frac{\partial^2\theta}{\partial y^2}\right)$$
 (5)

The boundary conditions used are

$$\frac{\partial u}{\partial y} = \frac{\partial v}{\partial y} = 0$$

$$p = p_{\infty} = 0$$
 and
$$\begin{cases} \frac{\partial \theta}{\partial y} = 0 & \text{if } v \ge 0 \\ \theta = 0 & \text{if } v < 0 \end{cases}$$
 at $y = 2H$ (6)

$$\frac{\partial u}{\partial x} = \frac{\partial v}{\partial x} = \frac{\partial \theta}{\partial x} = 0$$
 at $x = 0$ (7)

$$u = v = \frac{\partial \theta}{\partial x} = 0$$
 at $x = 1 + \kappa - \sqrt{\kappa^2 - H^2}$,

$$H < y < 2H \tag{8}$$

$$u = v = 0$$
 $\nabla \theta \cdot \mathbf{n} = 1$ at $1 \le x \le 1 + \kappa - \sqrt{\kappa^2 - H^2}$,

$$0 < y < H \tag{9}$$

At the inlet, the domain is extended as shown by the dotted line in Figure 1a, and the model for the inlet boundary condition proposed by Naylor et al. [31], which is based on treating the flow as a Jeffrey–Hamel flow [32], is adopted. With this approach, the flow at the extended inlet circular boundary is assumed to be normal at the boundary and directed toward the center point O in Figure 1a. Moreover, if this boundary is placed far enough from the heated wall, the temperature and radial stress can be set equal to the surrounding fluid temperature T_{∞} and zero, respectively. Mathematically this is expressed as

$$\mathbf{u} \cdot \mathbf{t} = -p + 2\nabla \mathbf{u} \cdot \mathbf{n} = 0 \text{ and } \theta = 0 \text{ for } x^2 + y^2 = 5^2,$$

$$x > 0, y < 0 \tag{10}$$

where \mathbf{n} and \mathbf{t} are unit vectors in the direction normal and tangential to the inlet circular boundary, respectively.

vol. 30 no. 14 2009

At the exit, the computational domain is not extended beyond the outlet section of the adiabatic extensions. In their study of natural convection heat transfer in parallel-plate channels using a stream function and vorticity formulation, Andreozzi et al. [22, 23] also extended the computational domain downstream of the outlet section of the adiabatic extensions in order to better estimate the edge effects at the system outlet zone. Since a primitive variable formulation is adopted in this work, the correct atmospheric pressure is imposed at the channel exit. When combined with the fact that the height of the adiabatic extensions considered in this work is equal to the height of the convex channel, inaccuracies at the outlet section will have negligible effects on the heated section.

SOLUTION PROCEDURE

The system of coupled conservation equations [Eqs. (2)–(5)] subject to the boundary conditions [Eqs. (6)–(10)] is numerically solved using a pressure-based finite-volume method. Solutions are obtained by subdividing the physical domain, depicted in Figure 1a, into a finite number of control volumes, each associated with a grid point placed at its geometric center (Figure 1d). The partial differential equations [Eqs. (2)-(5)] are integrated over each control volume, and profile approximations for the diffusion [33] and convection (the SMART scheme [34] applied within the context of the NVSF methodology [35] is used here) terms are made in each coordinate direction to replace the derivatives by algebraic expressions. The integral value of the source term over a control volume (Figure 1d) is evaluated by assuming the source at the control volume center to be equal to the mean value over the whole control volume. The resulting system of algebraic equations is then solved by a block Thomas algorithm [36]. To evaluate the pressure field, a pressure correction

p' (= $p - p^*$, where p^* is the solution from the previous iteration) is defined and a pressure correction equation is derived by combining the momentum and continuity equations as in the SIMPLE procedure of Patankar [36–38]. A collocated grid is used in the present study, and checkerboard pressure and velocity fields are suppressed through the use of the momentum weighted interpolation method (MWIM) while calculating the mass fluxes across the control volume faces [39].

Numerical Accuracy and Validation

Computations are performed using a mesh with 25,398 (83 \times 306) grid points. The grid points are unevenly distributed over the domain and concentrated near the walls where higher gradients are expected (Figure 1e). The grid independence of the results was verified by obtaining solutions in some selected cases ($\kappa=1,\ 10 \le Gr \le 10^4$) on a finer mesh with 57,360 (120 \times 478) grid points and comparing them to the predictions of the coarser mesh (25,398 grid points). The comparison revealed that the maximum differences in the average Nusselt number value and in the buoyancy-induced volume flow rate were less than 0.012% and 0.01%, respectively. Conservation of the various physical quantities was satisfied to within $10^{-6}\%$ in each control volume.

The accuracy of the solution procedure already described is established by comparing the average Nusselt number and volume flow rate results obtained in a vertical channel with similar ones reported by Lee [17] in Figure 2a. Noting that values from [17] were extracted from a small plot, the two solutions compare very well and are nearly identical.

As a further check for accuracy, numerical solutions are generated for natural convection heat transfer in a vertical channel asymmetrically heated at uniform heat flux, with adiabatic

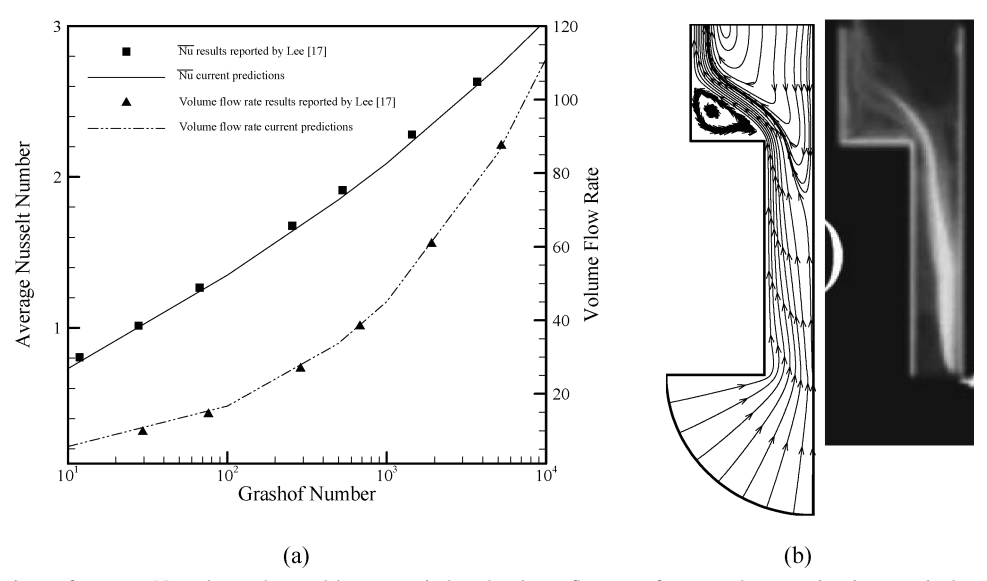


Figure 2 (a) Comparison of average Nusselt number and buoyancy-induced volume flow rate for natural convection in a vertical straight channel with the numerical data of Lee [17]. (b) Comparison of streamlines generated numerically with experimental ones reported in Manca et al. [19].

extensions (Figure 2b). One extension is coplanar to the unheated wall, while the other one is offset with respect to the heated wall, causing a sudden expansion of the channel. This problem was analyzed experimentally by Manca et al. [19] and results are obtained here for extension and expansion ratios of 1.5 and 2.5, respectively. The heat flux, the length of the heated wall, and the width of the channel are set at 300 w/m², 0.1 m, and 0.02 m, respectively. Computed streamlines are compared in Figure 2b with a snapshot of the flow field visualized experimentally [19] by injecting smoke at the channel inlet from the unheated side. As shown, the numerically generated flow field is very similar to the experimentally measured one with the cold inflow along the adiabatic wall captured correctly.

RESULTS AND DISCUSSION

The geometric parameters affecting the natural convection heat transfer in this study are the channel aspect ratio (i.e., channel height to channel width ratio), the channel extension ratio (i.e., heated channel height to extension height ratio), and the channel radius of curvature (κ), which is a measure of the channel expansion ratio. In order to limit the number of cases

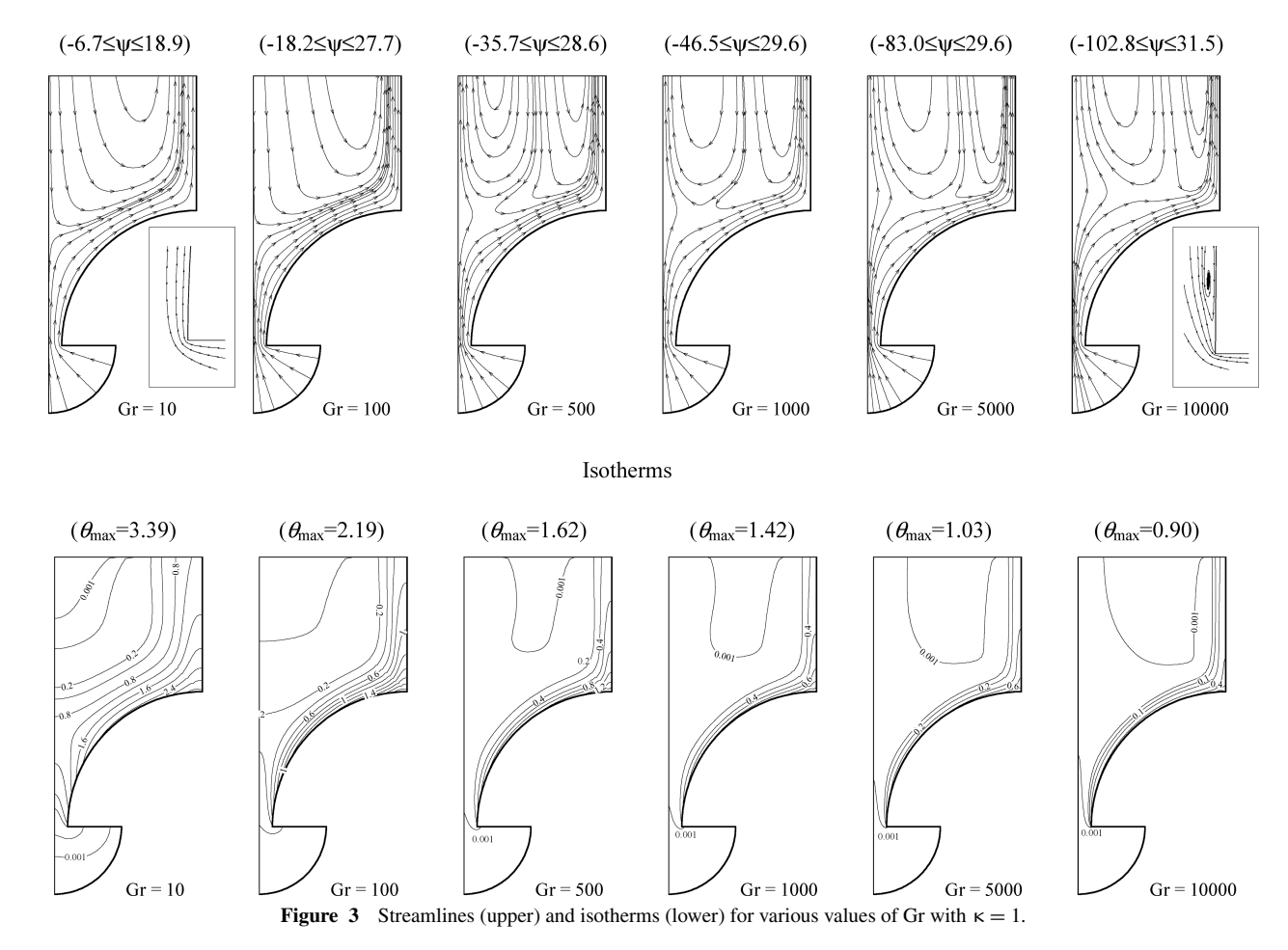
to be studied, the channel aspect and extension ratios are fixed at 10 and 1, respectively. The only geometric parameter that is varied is the channel radius of curvature, which is assigned 18 different values ($\kappa = 1, 1.025, 1.05, 1.075, 1.1, 1.15, 1.2, 1.25, 1.3, 1.35, 1.4, 1.45, 1.5, 2, 5, 20, 50, and <math>\infty$). On the other hand, the thermophysical parameters in the problem are reduced to the two dimensionless groups: the Grashof (Gr) and Prandtl (Pr) numbers. Air is considered to be the working fluid and, as such, the Prandtl number is assigned a value of 0.7 while the Grashof number is varied and assigned the following six values: Gr = 10, 10^2 , 5×10^2 , 10^3 , 5×10^3 , and 10^4 .

Results are presented in the form of streamlines, isotherms, mass flow rate estimates, local and average Nusselt numbers, and maximum wall temperature values.

Streamlines and Isotherms

The influence of Grashof number and hot wall curvature on the flow and temperature fields is revealed by the streamline and isotherm plots depicted in Figures 3–9. Figures 3 through 5 show the effect of Grashof number on natural convection for given values of the hot wall radius of curvature. Figures 6 through

Streamlines



heat transfer engineering

Streamlines

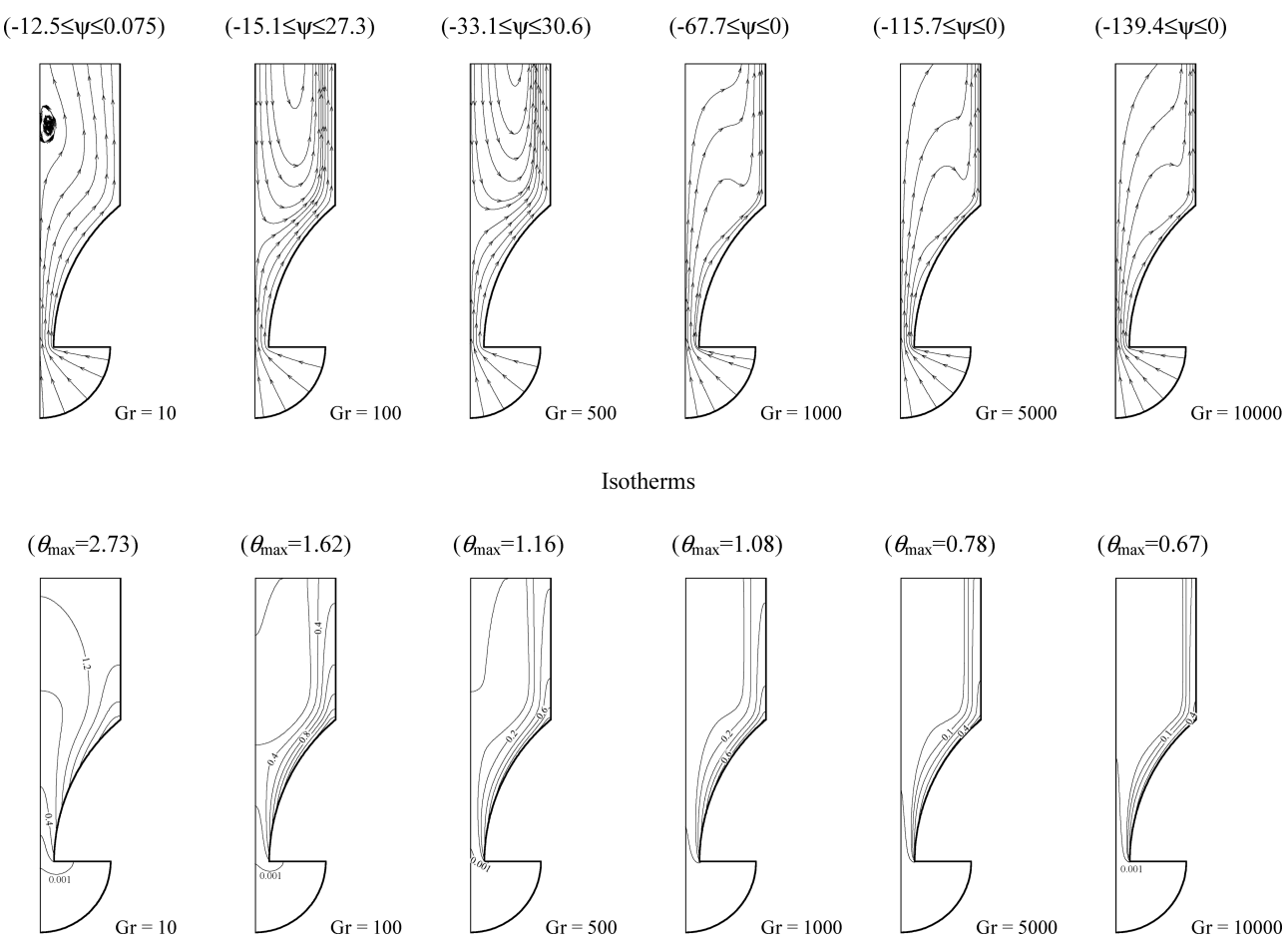


Figure 4 Streamlines (upper) and isotherms (lower) for various values of Gr with $\kappa = 1.3$.

9 reveal the effect of the hot wall radius of curvature on heat transfer at a given Grashof number. Above each streamline map, the range of the stream function over the domain is displayed. Because the minimum value of θ is zero, only the maximum value of temperature is displayed on the top of the isotherm maps.

At the smallest radius of curvature considered (i.e., $\kappa=1$), for which the convex wall represents a quarter of a circle and the expansion ratio is 10, the streamlines presented in Figure 3 reveal recirculation in the exit section at all values of Grashof number. In general, the buoyancy-induced flow drifts toward the hot wall and follows its curved contour. At low Grashof number values (Gr $\leq 10^2$), one recirculation zone occurs in the exit section with the recirculating fluid entering along the central portion of the domain and leaving along the insulated wall. At low values of Gr, buoyancy effects at the end of the expanded section and near the axis of symmetry are not strong enough to overcome the slowing-down effect of channel expansion, which leads to the formation of one recirculation zone with the recirculating flow entering in the region surrounding the axis of symmetry and leaving with the primary flow along the region

with the largest buoyancy effect, which is the curved (heated) channel wall followed by the insulated wall. For $Gr \ge 5 \times 10^2$, two recirculation zones are present in the exit section where the entrained flow enters along the middle of the exit section and splits into two parts; one part leaves the channel along the axis of symmetry, while the remaining part leaves along the insulated wall. In this case, the primary flow through the channel inlet is also split into two parts, with one part leaving along the axis of symmetry and the other part along the insulated wall. The switching from one to two recirculation zones in the exit section as Gr exceeds a threshold value (somewhere between 100 and 500) is an adaptation of the flow field in response to stronger buoyancy effects enabling the flow near the axis of symmetry to overcome the opposing pressure gradient imposed by the expansion of the channel. If the primary flow leaves along the two streamlines coinciding with the channel wall on the right and the axis of symmetry on the left, then the entrained flow, if it exists, must enter somewhere between these two streamlines, causing two recirculation zones to occur. Whether the entrained flow exists or not is again decided by the interplay between the buoyancy force pushing the fluid upward and the opposing positive

Gr = 10000

Streamlines

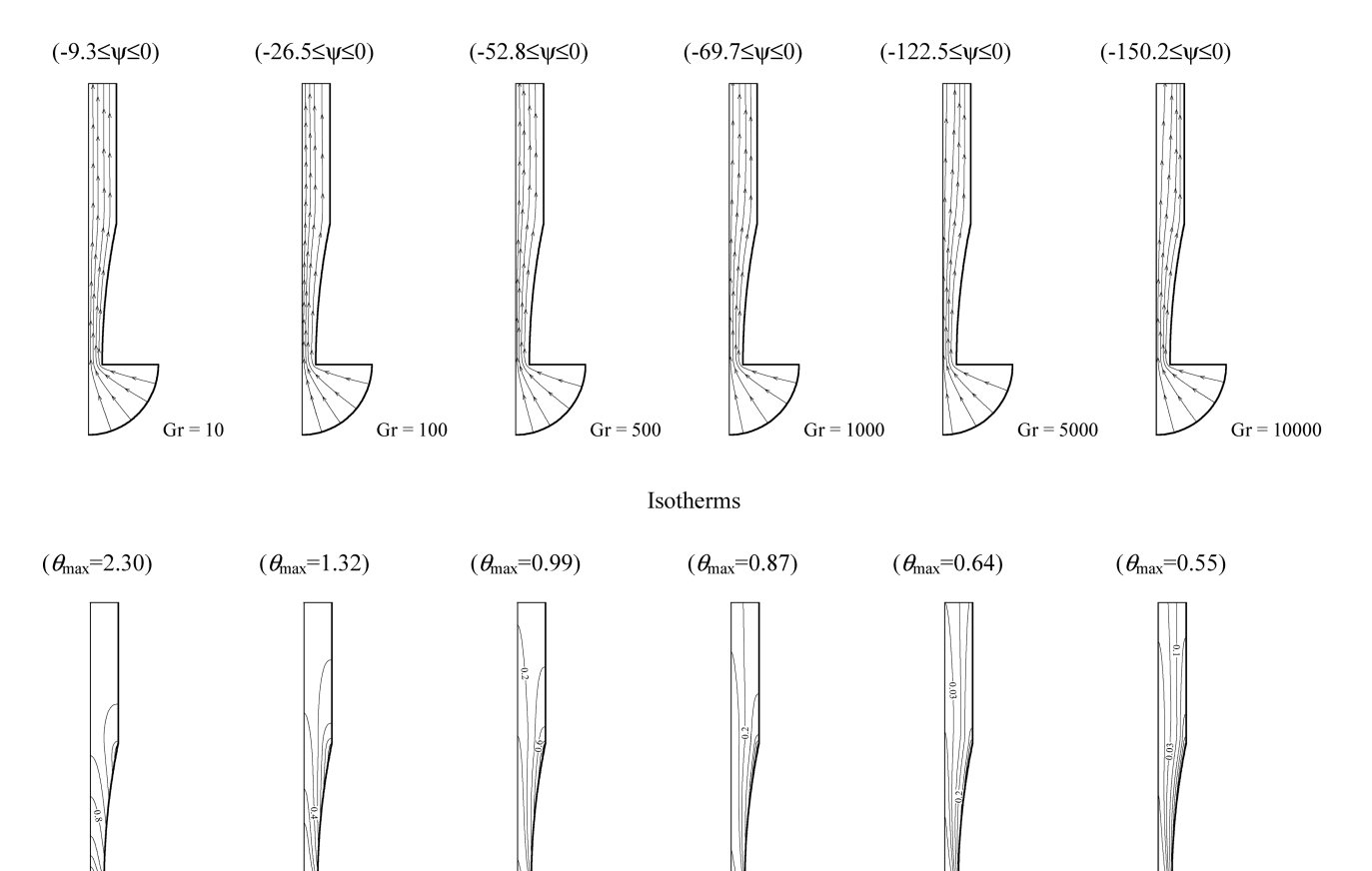


Figure 5 Streamlines (upper) and isotherms (lower) for various values of Gr with $\kappa = 5$.

Gr = 500

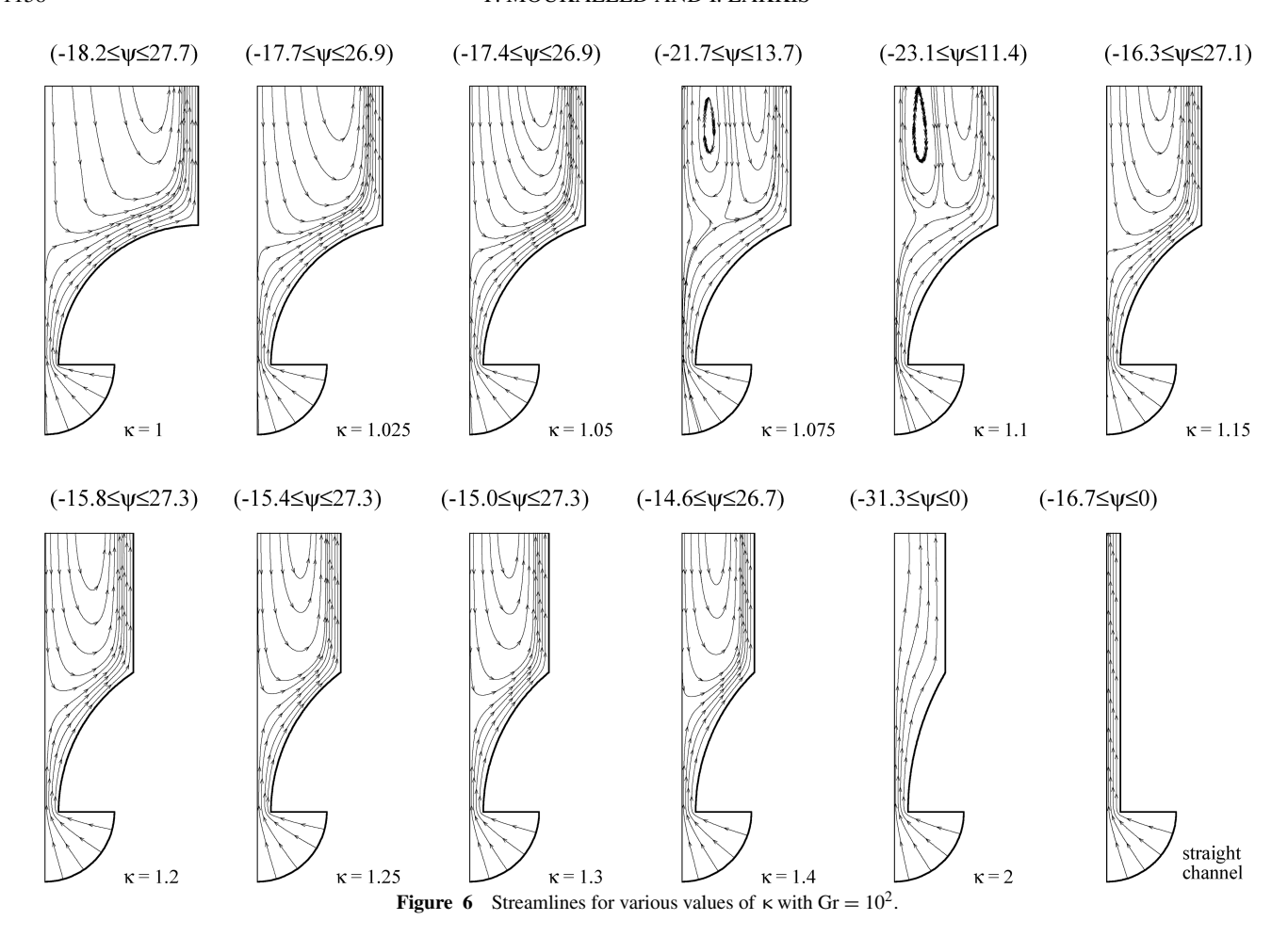
Gr = 1000

pressure gradient induced by expansion of the channel. Moreover, the range of stream function values displayed in Figure 3 indicates an increase in the strength of both the primary and recirculating flows with increasing values of Grashof number due to stronger buoyancy effects. For Gr=10 and 10^4 , a small plot magnifying the inlet region to the channel is presented. As depicted in Figure 3, no recirculation is noticed when Gr=10 while a recirculation zone is formed at $Gr=10^4$, which is in accord with predictions reported by Naylor et al. [31] for natural convection in a vertical channel and by Lakkis and Moukalled [30] for natural convection in a channel with an isothermally heated convex surface.

The increase in buoyancy effects with increasing Grashof number values is further demonstrated by the isotherms displayed in Figure 3. At Gr = 10, the uniform distribution of isotherms and the relatively high diffusion of heat upstream from the heated section indicate dominant conduction heat transfer mode. As Gr increases, upstream diffusion decreases and isotherms become more clustered indicating stronger convection effects. At all values of Grashof number, temperature contours imitate the flow field with the recirculation zones in the

exit section clearly reflected in the distribution of isotherms. Because the dimensionless temperature θ is inversely proportional to Grashof number, as can be inferred from the definitions of θ and Gr, its maximum value θ_{max} over the domain, which occurs on the heated convex wall, decreases as Grashof number increases. The maximum dimensional temperature, however, increases with Grashof number as it is proportional to the product

Results for a channel with an expansion ratio of nearly 5.7 (i.e., $\kappa=1.3$) are presented in Figure 4. The streamlines displayed in the figure show that one recirculation zone is present in the exit section for Grashof number values less than 10^3 , while no recirculation ensues at $Gr \geq 10^3$. This is contrary to the results reported in [30], for the isothermal wall boundary condition, where recirculation in the exit section occurred at high values of Grashof number. At low Grashof number values, buoyancy effects are not strong enough and consequently the flow away from the hot wall cannot overcome the hydrodynamic effects resulting from the pressure increase due to the gradual expansion of the channel. As Grashof number increases, the buoyancy forces increase in strength and become capable of



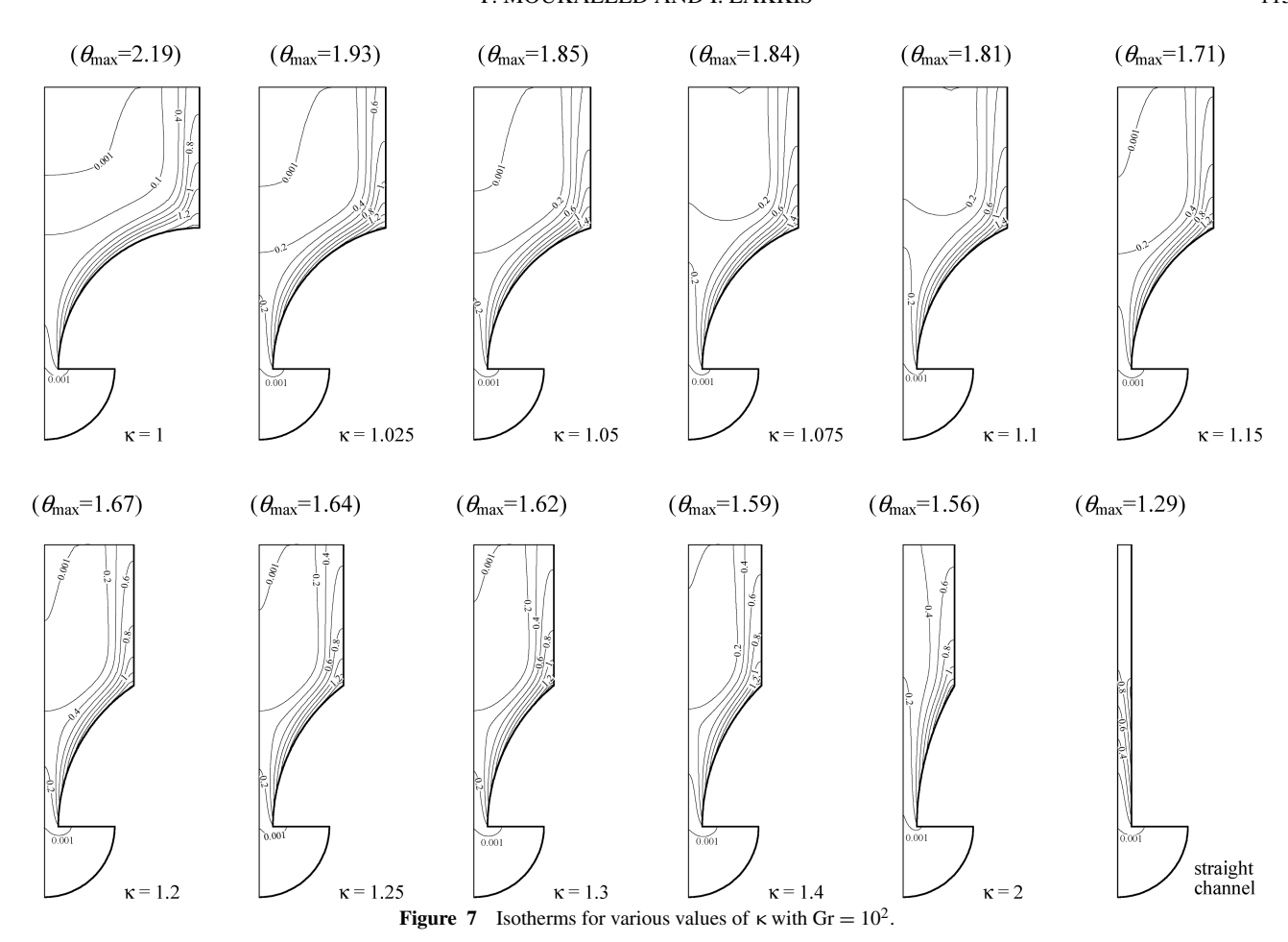
overcoming the slowing down effects of the positive pressure gradient. In all cases, most of the entrained flow drifts toward the hot wall and continues rising along the insulated vertical wall. Again, the range of stream function values displayed in the figure indicates an increase in the flow strength with increasing values of Grashof number.

At Gr = 10, isotherms presented in Figure 4 are uniformly distributed and the upstream diffusion is considerable, which indicates that conduction is the dominant heat transfer mode. As Gr increases, isotherms become more clustered close to the wall, signaling a higher contribution of convection to the total heat transfer. This is demonstrated by the decrease in the maximum temperature θ_{max} as Grashof number increases. As discussed earlier, larger Gr leads to a larger dimensional temperature which is proportional to $\theta\times$ Gr because the enhancement in convection heat transfer at larger Gr values is not large enough to offset the increase in temperature due to the larger heat flux at the wall.

Results presented in Figure 5 are for a channel with a radius of curvature of 5 (i.e., $\kappa=5$). For this configuration, the rate of expansion is small (\approx 2) and the effects of adverse pressure gradient over the curved surface are smaller than the buoyancy effects at all values of Grashof number. Consequently, no recirculation exists for any of the cases studied and the maximum

absolute value of the stream function increases from 9.3 at Gr = 10 to 150.2 at Gr = 10^4 . The isotherms of Figure 5 indicate that conduction is dominant at low Gr values with convection effects increasing with increasing values of Grashof number. Moreover, θ_{max} decreases from 2.3 at Gr = 10 to 0.55 at Gr = 10^4 . This rate of decrease in θ_{max} is lower than the rate of increase in Gr with a consequent increase in the maximum dimensional heated wall temperature.

Results displayed in Figures 6-9 demonstrate the curvature effects of the heated wall on the hydrodynamic and thermal fields for $Gr = 10^2$ (Figures 6 and 7) and $Gr = 10^4$ (Figures 8 and 9). For $Gr = 10^2$ (Figure 6), recirculation in the exit section occurs at κ < 1.4. For lower expansion ratios (i.e., κ > 1.4) the flow is buoyancy dominated so that it fills the entire channel cross section, inhibiting the formation of any recirculation zone. The effect of recirculation for $\kappa \leq 1.4$ on the isotherms presented in Figure 7 shows that the temperature inside the recirculation zone is approximately equal to that of the ambient fluid. For this Gr value, convection effects are low, as revealed by the uniform spread of isotherms over the domain and the upstream diffusion of heat at the inlet to the heated channel section. Moreover, the maximum dimensionless wall temperature decreases from a value of 2.19 at $\kappa = 1$ to 1.29 at $\kappa = \infty$. This is expected because the heated length of the channel decreases



as κ increases. Because the Grashof number is constant, the dimensional temperature $T_{\rm max}$ also decreases as κ increases in the same manner as θ_{max} . For $Gr = 10^4$, the streamline maps displayed in Figure 8 show the formation of two recirculation zones in the exit section of channels for which κ < 1.15. At $\kappa = 1$, the strength of the buoyant flow moving through the exit section is not great enough to overcome the adverse pressure gradient throughout the entire section. In this case, the rising fluid split into two streams, with one flowing over the hot curved wall and then along the insulated vertical wall, while the other moving vertically upward and leaving along the centerline of the channel. As the expansion ratio of the channel decreases (i.e., $1 < \kappa < 1.2$), the strength of buoyancy causes the flow entering the domain from the bottom section to drift toward the hot curved wall and then to move in its vicinity and along the insulated wall until it is discharged. For $\kappa < 1.2$, two recirculation zones are formed in the exit section, with their shape dictated by the difference between the strength of buoyancy and pressure gradient. The stream function values presented in the figure indicate that the strongest recirculation occurs at $\kappa = 1.05$. At higher values of κ (i.e., at lower expansion ratio, $\kappa > 1.15$) the flow through the expanded section is buoyant enough to fill the entire channel exit section without recirculation. The strength of convection heat transfer manifests itself by the dense clustering

of isotherms close to the hot surface. The packing of isotherms decreases as the fluid moves along the hot wall (showing boundary layer behavior); the decrease is higher at lower κ values due to the longer distance the fluid has to travel. As depicted in Figure 9, the maximum dimensionless wall temperature decreases from a value of 0.9 at $\kappa=1$ to 0.48 at $\kappa=\infty$. As the Grashof number remains constant, the dimensional temperature also decreases as κ increases for the same reasons as stated earlier.

In comparison with results presented in [30], for the isothermal wall boundary condition, the hydrodynamic and heat transfer characteristics of the buoyancy-induced flow predicted here are different. Although for some of the configurations studied in [30] separation of the flow moving along the concave surface was reported with ambient recirculating air reaching the concave surface, no separation is predicted for the uniform heat flux cases analyzed in this work. Even though recirculation occurs in the exit section, the entrained flow always drifts towards the hot wall and continues rising along the insulated vertical wall. This behavior of the buoyancy-induced flow has a profound influence on the temperature field, and consequently the system's heat transfer characteristics, and justifies the need for undertaking the current investigation.

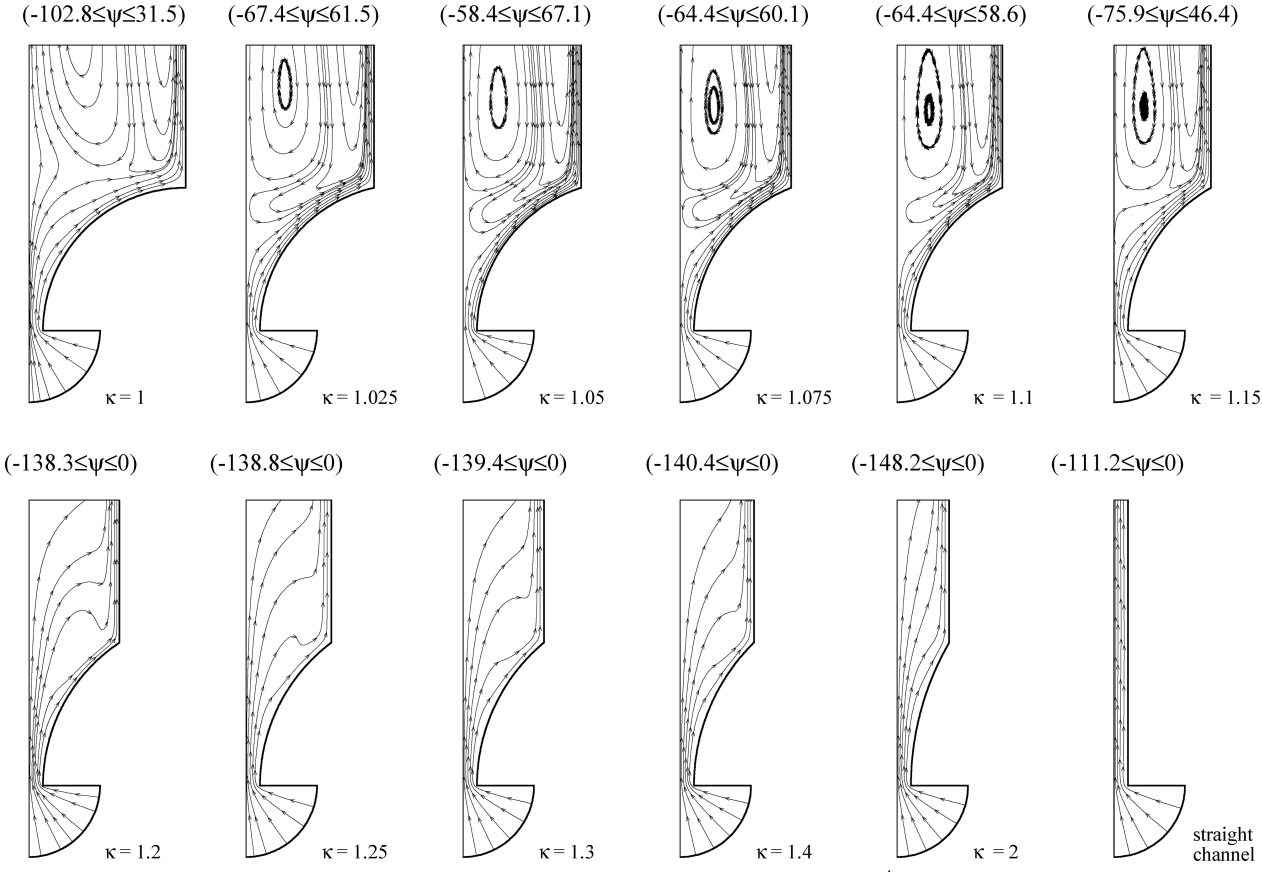


Figure 8 Streamlines for various values of κ with $Gr = 10^4$.

Volume Flow Rates

Another hydrodynamic parameter of interest in this study is the dimensionless volume flow rate \mathcal{Q} (for half the channel), which is calculated at the inlet to the channel as

$$Q = \int_{\mathbf{S}} \mathbf{u} \cdot d\mathbf{s} \tag{11}$$

The volume flow rates obtained using this equation are multiplied by $Gr^{1/2}$ to get the actual strength (Q $Gr^{1/2}$) and are plotted in Figure 10 as a function of κ for different values of Grashof number. At all values of the expansion ratio κ , plots indicate an increase in the buoyancy-induced volume flow rate with increasing Gr values due to the acceleration of the flow along the heated curved wall. As shown in Figure 10, variations of the volume flow rates with κ at a given Gr are highly nonlinear for $\kappa \leq 1.5$. This nonlinearity is attributed to the combined effects of the channel expansion ratio and the buoyancy forces on the flow field. A decrease in κ is associated with an increase in the length of the heated wall, with a consequent increase in buoyancy forces that drive the flow. On the other hand, a decrease in k results in an increase in the expansion of the channel, resulting in a decrease in velocity and a corresponding increase in pressure. Depending on whether the increase in the flow velocity in the thermal boundary layer overwhelms the decrease in the

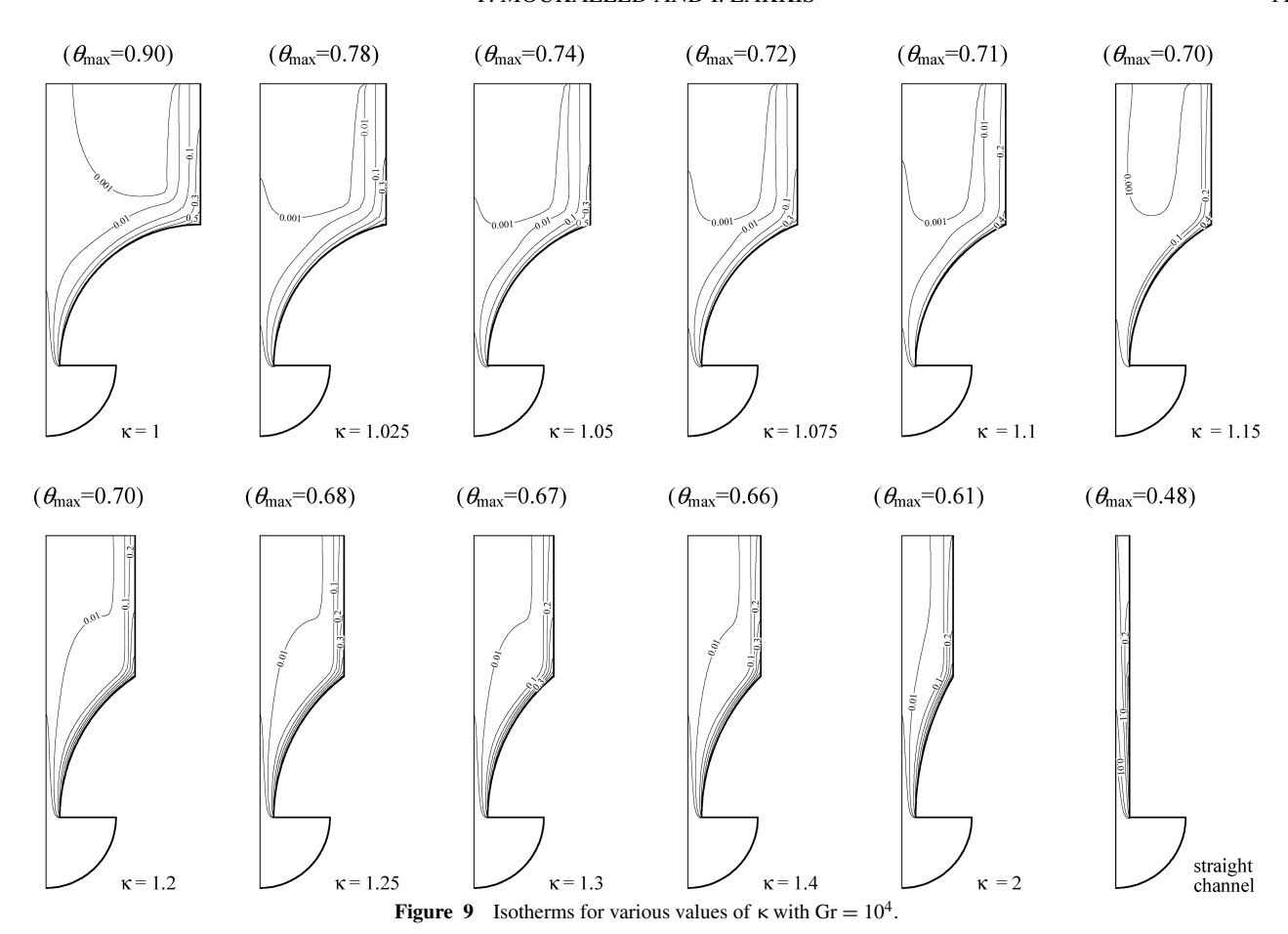
flow velocity due to the expansion of the channel, the volume flow rate could either decrease or increase when κ varies, as depicted in Figure 10. For $\kappa > 1.5$, Q Gr^{1/2} decreases with increasing κ values, for a given Gr, due to a decrease in buoyancy forces resulting from the reduced length of the curved heated wall.

Convex Wall Temperatures and Nusselt Numbers

The predicted wall temperatures are plotted in Figure 11 as a function of y, the location along the vertical height of the heated convex wall. In these plots, values of $\theta_w \times$ Gr rather than θ_w are used in order to demonstrate the actual variation in the dimensional temperature. Figures 11a and 11b show the effect of varying Grashof number on temperature profiles, while Figures 11c and 11d reveal the influence of the hot wall radius of curvature. Plots in Figures 11a and 11b are for radii of curvature (κ) of values 1 and 5, respectively. For both κ values, the wall temperature level increases with increasing Gr number due to a greater heat flux. At any Gr value, the wall temperature increases as γ increases due to the increase in the fluid temperature while moving over the curved section of the hot wall. This increase is explained as follows: With the heat flux being uniformly distributed over the hot wall and the diffusion coefficient being

heat transfer engineering

vol. 30 no. 14 2009



constant, the normal gradient along the curved wall should remain constant. Because the fluid is continuously heated while moving along the hot wall, its temperature increases. Thus for the normal gradient to remain constant, the wall temperature has to increase in the streamwise direction. Curves presented in Figures 11c and 11d indicate a similar trend in results for both Gr values with temperature profiles packing themselves in two clusters. For $Gr = 10^2$ transition between the two clusters occurs at $\kappa = 2$, while it takes place at $\kappa = 5$ for $Gr = 10^4$. The level of temperature profiles increases with decreasing κ values due to an increase in the length of the hot wall. The large increase in temperature for $\kappa = 1$ near the edge of the hot wall is due to the large change in the flow direction (from horizontal to vertical) while negotiating the corner, the increase in the boundary layer thickness (associated with a decrease in the average velocity in the boundary layer), and the increase in the temperature of the fluid by upstream heating.

An important design parameter is the maximum temperature occurring over the hot wall. These temperatures are multiplied by Gr and plotted as a function of κ at different Grashof number values in Figure 12a. At a given κ value, $\theta_{max}\times$ Gr estimates increase with increasing Gr values due to greater heat flux. Moreover, at a given Grashof number, $\theta_{max}\times$ Gr values maximize at $\kappa=1$ for which the length of the heated wall is maximum, as stated earlier. Moreover, the value of κ at which

the temperature is minimum increases with Grashof number (i.e., $\kappa = 5$ at Gr = 100 and $\kappa = 50$ at $Gr = 10^4$). For $Gr \ge 100$, θ_{max} Gr values plotted in Figure 12a are correlated with a maximum absolute error of less than 5.6% ($r^2 = .995$) using

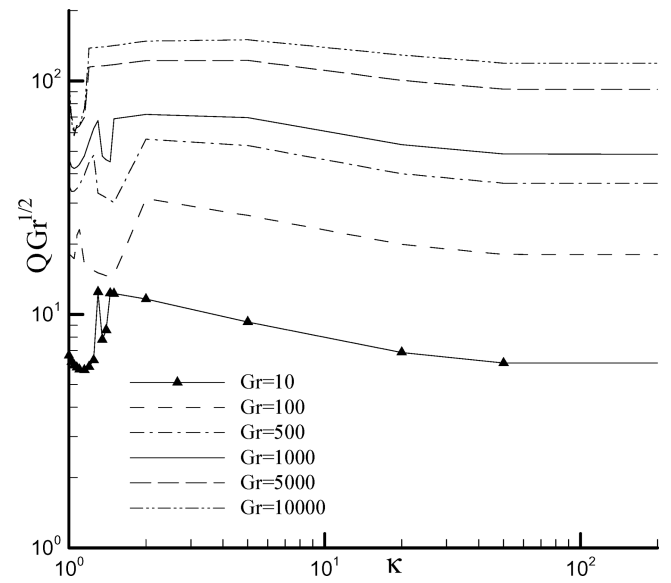


Figure 10 Variation of buoyancy-induced volume flow rate with κ at different Gr values.

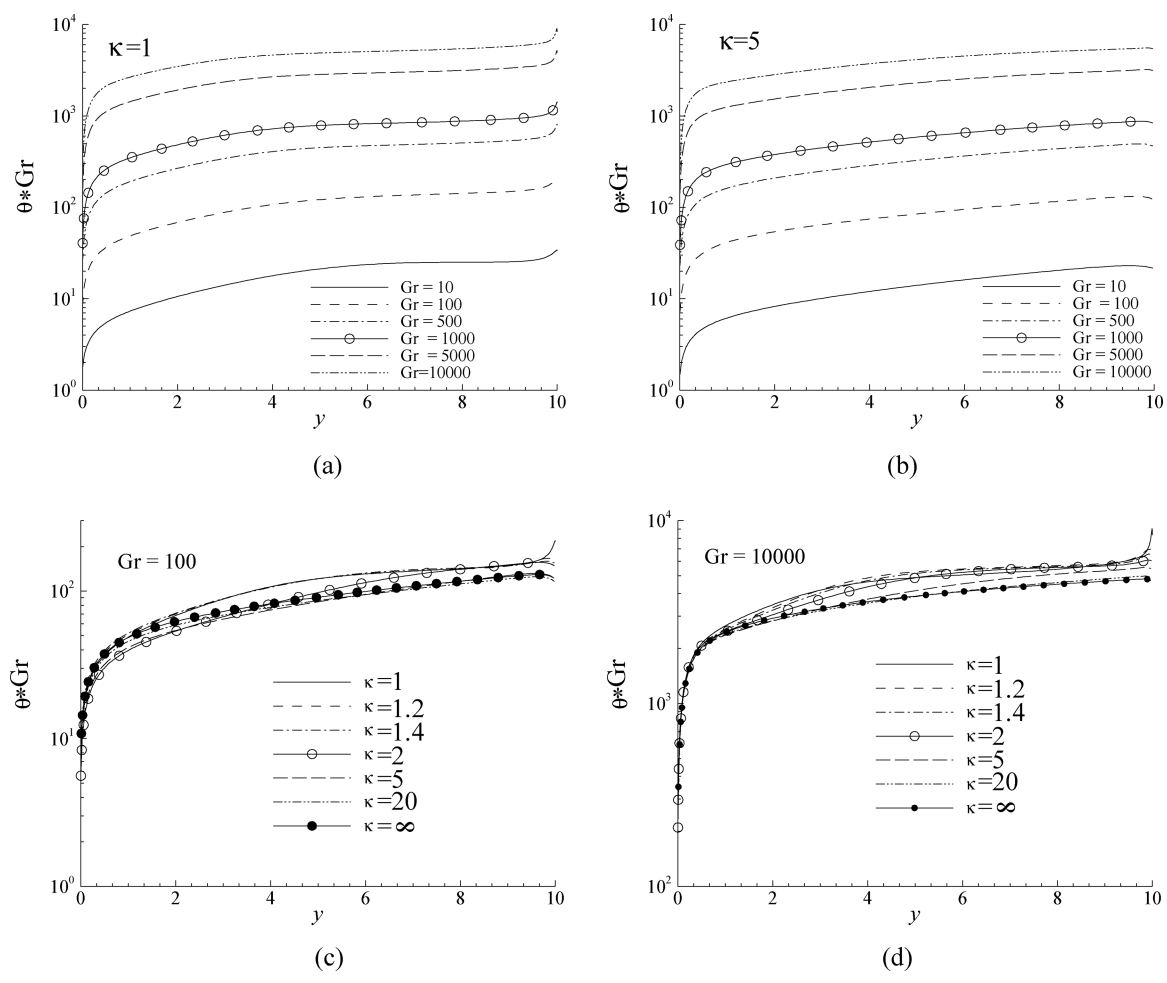


Figure 11 Curved wall temperature variation with y for different Gr values at (a) $\kappa = 1$ and (b) $\kappa = 5$ and for different κ values at (c) $Gr = 10^2$ and (d) $Gr = 10^4$.

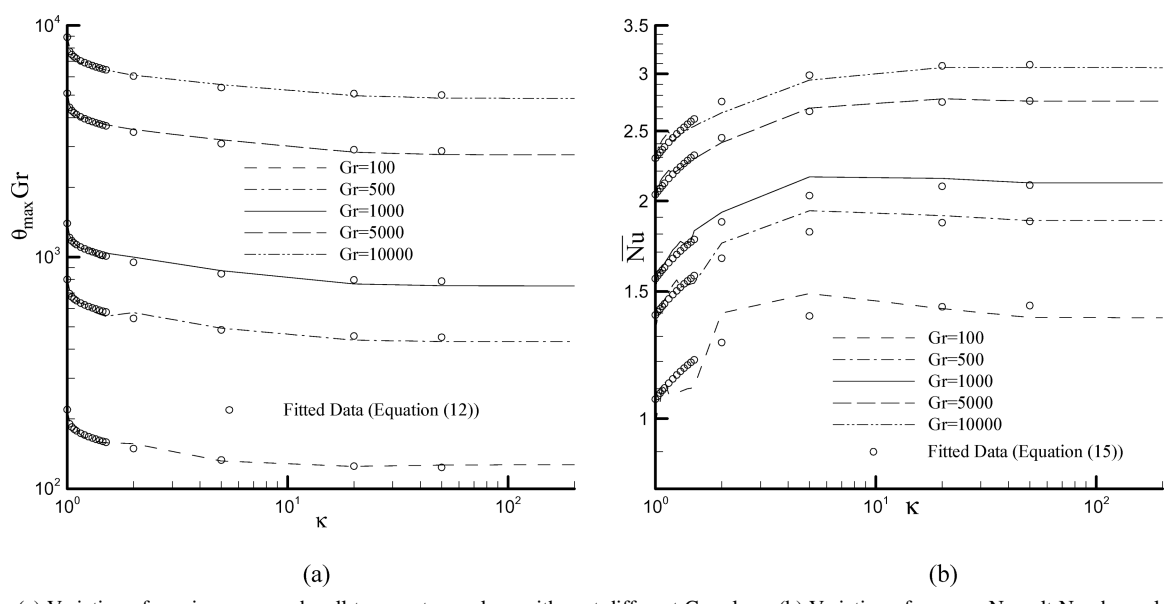


Figure 12 (a) Variation of maximum curved wall temperature values with κ at different Gr values. (b) Variation of average Nusselt Number values with κ at different Gr values.

the following equation:

$$\theta_{max} * Gr = 3.445 * (Gr)^{0.804}$$

$$\times \left[\left(\frac{1.753}{\sinh\left(1 + \frac{1}{\kappa}\right)} \right)^{7.449} - \frac{0.016}{\sinh\left(1 + \frac{1}{\kappa}\right)} \right]^{-0.044}$$
 (12)

For comparison, estimates generated using Eq. (12) are displayed in Figure 12a along with the computed values.

Another heat transfer parameter of interest is the Nusselt number (Nu). The local and average Nusselt number values along the heated curved wall are calculated as

$$Nu = hw/k \qquad \overline{Nu} = \frac{1}{\ell} \int_{0}^{\ell} Nu \, d\ell$$
 (13)

where w is the width of the channel at the inlet. Moreover, the heat transfer coefficient h is defined as

$$h = \frac{k}{w} \frac{1}{\theta_w} \underbrace{\nabla \theta_w \cdot \mathbf{n}}_{=1} \implies \text{Nu} = \frac{1}{\theta_w}$$
 (14)

Because $Nu = 1/\theta_w$, variations in the local Nusselt number may be deduced from plots of θ_w shown in Figure 11. Average Nusselt number values are plotted as a function of κ at different Grashof and presented in Figure 12b. At a given κ value, Nuincreases as Gr increases due to increased heat flux. Variations with κ for a given Gr show local minima and maxima at low κ values. Moreover, at a given Grashof number, \overline{Nu} is maximized at a k value that increases with increasing Gr. Based on Eqs. (13) and (14), the two parameters that control the value of \overline{Nu} are the wall temperature and the length of the hot wall, which are both related to κ . Since the heat flux at any location along the heated wall is constant, the wall temperature distribution is dictated by the temperature of the air in its vicinity, which is greatly affected by the recirculation zone that may form in the exit section. If recirculation occurs, it entrains colder fluid into the channel leading to a lower wall temperature (\dot{q}_w is constant) with a consequent increase in Nu. Similarly, an increase in the expansion ratio is associated with an increase in the length of the hot wall with a consequent decrease in the average Nusselt number. The combined influence of the wall temperature and the length of the hot wall may cause Nu to either increase or decrease resulting in the distribution shown in Figure 10b. Since at large κ values no recirculation occurs and the length of the hot wall is nearly equal to that of a straight channel, \overline{Nu} remains nearly constant. For Gr ≥ 100 , \overline{Nu} values plotted in Figure 12b are correlated to Gr and K, with a maximum absolute error of less than 8.8% ($r^2 = .991$) using the following equation:

$$\overline{Nu} = \frac{2}{3}Gr^{1/6}e^{-0.3/\kappa^{4/3}}$$
 (15)

For comparison, estimates generated using Eq. (15) are displayed in Figure 12b along with the computed values.

CLOSING REMARKS

This article reported on a numerical investigation conducted to study laminar natural convection heat transfer in channels with isoflux convex surfaces. At a small radius of curvature ($\kappa \leq 1.15$), results revealed the formation of one or two recirculation zones in the exit section of the channel. At a higher radius of curvature, one or no recirculation zone was observed and the value of Grashof number at which recirculation occurred increased until it disappeared at k values greater than 2. Variations in the buoyancy-induced volume flow rates were found to be highly nonlinear as a result of the competing effects of the channel expansion ratio and the buoyancy forces. Moreover, it was found that the radius of curvature (κ) at which the volume flow rate is maximum increases with increasing Gr. The value of κ at which θ_{max} Gr is minimum increases with Grashof number. At low Grashof number values ($Gr \le 10^2$) the maximum temperature is minimized in a channel with $\kappa = 5$, whereas it is minimized in a channel with $\kappa = 20$ for $Gr = 5 \times 10^2$ and 10^3 , and $\kappa = 50$ for $Gr = 5 \times 10^3$ and 10^4 . The local Nusselt number along the channel decreases in the direction of the flow due to the fact that the wall temperature increases in a boundary layer flow over a surface with constant heat flux. For all configurations studied the average Nusselt number (\overline{Nu}) increases with increasing Grashof number values.

NOMENCLATURE

specific heat

$\sim p$	specific near
g	gravitational acceleration
Gr	Grashof number (= $g \beta \rho^2 \dot{q}_w w^4 / \mu^2 k$)
h	convection heat transfer coefficient
Н	height of curved channel section and of channel ex-
	tension
k	fluid thermal conductivity
ℓ	dimensionless length of hot wall
Nu	local Nusselt number
\overline{Nu}	average Nusselt number
P	dimensional pressure
p	dimensionless pressure
p_{∞}	surrounding pressure

Pr	Prandtl number (=
\dot{q}_w	wall heat flux
Q	volume flow rate
R	radius of curvature
•	

regression coefficient of determination

s surface vector

T dimensional temperature

 $T_{
m max}$ maximum dimensional temperature $T_{
m \infty}$ dimensional surrounding temperature

 $T_{
m w}$ dimensional wall temperature u, v dimensionless velocity components U, V dimensional velocity components

w channel inlet widthx, y dimensionless coordinatesX, Y dimensional coordinates

Greek Symbols

β thermal expansion coefficient

μ dynamic viscosity

ρ density

θ dimensionless temperature

 θ_{max} maximum dimensionless temperature

 θ_w dimensionless wall temperature

ψ stream function

κ dimensionless radius of curvature

REFERENCES

- [1] Elenbaas, W., Heat Dissipation of Parallel Plates by Free Convection, *Physica*, vol. 9, pp. 1–28, 1942.
- [2] Bodoia, J. R., and Osterle, J. F., The Development of Free Convection Between Heated Vertical Plates, ASME Journal of Heat Transfer, vol. 84, pp. 40–44, 1962.
- [3] Aung, W., Fletcher, L. S., and Sernas, V., Developing Laminar Free Convection between Vertical Flat Plates with Asymmetric Heating, *International Journal of Heat Mass Transfer*, vol. 15, pp. 2293–2308, 1972.
- [4] Sparrow, E. M., Chrysler, G. M., and Azevedo, L. F., Observed Flow Reversals and Measured-Predicted Nusselt Numbers for Natural Convection in a One-Sided Heated Vertical Channel, ASME Journal of Heat Transfer, vol. 106, pp. 325–332, 1984.
- [5] Nieckle, A. O., and Azevedo, L. F. A., Reverse Flow in One-Sided Heated Vertical Channels in Natural Convection, Winter Annual Meeting of the ASME, pp. 71–77, Boston, 1987.
- [6] Haaland S. E., and Sparrow, E. M., Solutions for the Channel Plume and the parallel-Walled Chimney, *Numer. Heat Transfer*, vol. 6, pp. 155–172, 1983.
- [7] Kihm, K. D., Kim, J. H., and Fletcher, L. S., Investigation of Natural Convection Heat Transfer in Converging Channel Flows Using a Specklegram Technique, ASME Journal of Heat Transfer, vol. 115, pp. 140–148, 1993.
- [8] Said, S. A. M., Investigation of Natural Convection in Convergent Vertical Channels, *International Journal of Energy Research*, vol. 20, pp. 559–567, 1996.
- [9] Kaiser, A. S., Zamora, B., and Videma, A., Correlation for Nusselt Number in Natural Convection in Vertical Convergent Channels at Uniform Wall Temperature by a Numerical Investigation, *In*ternational Journal of Heat Fluid Flow, vol. 25, pp. 671–682, 2004.
- [10] Marcondes, F., Melo, V. S., and Gurgel, J. M., Numerical Analysis of Natural Convection in Parallel, Convergent, and Divergent Open-Ended Channels, *International Journal of Numerical Methods of Heat and Fluid Flow*, vol. 16, pp. 304–323, 2006.
- [11] Langellotto, L., Manca, O., and Nardini, S., Numerical Investigation of Transient Natural Convection in Air in a Convergent Vertical Channel Symmetrically Heated at Uniform Heat Flux, *Numerical Heat Transfer A*, vol. 51, pp. 1065–1086, 2007.

- [12] Sparrow, E. M., and Ruiz, R., Experiments on Natural Convection in Divergent Vertical Channels and Correlation of Divergent, Convergent, and Parallel-Channel Nusselt Numbers, *International Journal of Heat Mass Transfer*, vol. 31, pp. 2197–2205, 1988.
- [13] Shalash, J. S., Tarasuk, J. D., and Naylor, D., Experimental and Numerical Studies of Natural Convection Heat Transfer in Vertical Converging Channel Flows, *Proc. 4th Experimental Heat Trans*fer, Fluid Mechanics and Thermodynamics Conference, Brussels, Belgium, pp. 2167–2174, 1997.
- [14] Straatman, A. G., Tarasuk, J. D., and Floryan, J. M., Heat Transfer Enhancement from a Vertical, Isothermal Channel Generated by the Chimney Effect, ASME Journal of Heat Transfer, vol. 115, pp. 395–402, 1993.
- [15] Auletta, A., Manca, O., Morrone, B., and Naso, V., Heat Transfer Enhancement by the Chimney Effect in a Vertical Isoflux Channel, *International Journal of Heat Mass Transfer*, vol. 44, pp. 4345– 4357, 2001.
- [16] Manca, O., Musto, M., and Naso, V., Experimental Analysis of Asymmetrical Isoflux Channel-Chimney Systems, *International Journal of Thermal Sciences*, vol. 42, pp. 837–846, 2003.
- [17] Lee, K. T., Natural Convection in Vertical Parallel Plates With an Unheated Entry or Unheated Exit, *Numerical Heat Transfer A*, vol. 25, pp. 477–493, 1994.
- [18] Manca, O., Musto, M., and Naso, V., Experimental Analysis of Chimney Effect in a Vertical Isoflux Channel, *Proc. 5th World Conf. on Experimental Heat Transfer, Fluid Dynamics, and Ther-modynamics*, pp. 645–650, Thessaloniki, Greece, 2001.
- [19] Manca, O., Musto, M., and Naso, V., Experimental Investigation of Natural Convection in an Asymmetrically Heated Vertical Channel With an Asymmetric Chimney, ASME Journal of Heat Transfer, vol. 127, pp. 888–896, 2005.
- [20] Auletta, A., and Manca, O., Heat and Fluid Flow Resulting from the Chimney Effect in a Symmetrically Heated Channel With Adiabatic Extensions, *International Journal of Thermal Sciences*, vol. 41, pp. 1101–1111, 2002.
- [21] Campo, A., Manca, O., and Marrone, B., Numerical Analysis of Partially Heated Vertical Parallel Plates in Natural Convective Cooling, *Numerical Heat Transfer A*, vol. 36, pp. 129–151, 1999.
- [22] Andreozzi, A., Buonomo, B., and Manca, O., Numerical Study of Natural Convection in vertical channels with adiabatic extensions downstream, Numerical Heat Transfer A Applications, vol. 47, pp. 74–762, 2005.
- [23] Andreozzi, A., Campo, A., and Manca, O., Compounded Natural Convection Enhancement in a Vertical Parallel-Plate Channel, *International Journal of Thermal Science*, vol. 47, pp. 742–748, 2008.
- [24] Pop, I., and Takhar, H. S., Free Convection From a Curved Surface, Journal of Applied Mathematics and Mechanics (ZAMM), vol. 73, pp. 534–539, 1993.
- [25] Magyari, E., Pop, I., and Keller, B., A Note on the Free Convection From Curved Surfaces, *Journal of Applied Mathematics and Mechanics* (ZAMM), vol. 82, pp. 142–144, 2002.
- [26] Nakayama, A., Koyoma, H., and Kuwahara, F., Similarity Solution for Non-Darcy Free Convection From a Non-isothermal Curved Surface in a Fluid-Saturated Porous Medium, *Journal of Heat Transfer*, vol. 111, pp. 807–811, 1989.
- [27] Char M. C., and Chang, C. L., Laminar Free Convection Flow of Mircopolar Fluids from a Curved Surface, *Journal of Physics D: Applied Physics*, vol. 28, pp. 1324–1331, 1995.

- [28] Moukalled, F., Doughan, A., and Acharya, S., Mixed-Convection Heat Transfer in Concave and Convex Channels, AIAA Journal of Thermophysics and Heat Transfer, vol. 13, no. 4, pp. 508–516, 1999.
- [29] Moukalled, F., Doughan, A., and Acharya, S., Parametric Study of Mixed Convection in Channels With Concave and Convex Surfaces, *International Journal of Heat Mass Transfer*, vol. 43, pp. 1947–1963, 2000.
- [30] Lakkis, I., and Moukalled, F., Natural-Convection Heat Transfer in Channels With Isothermally Heated Convex Surfaces, *Numer. Heat Transfer A*, vol. 53, pp. 1176–1194, 2008.
- [31] Naylor, D., Floryan, J. M., and Tarasuk, J. D., A Numerical Study of Developing Free Convection Between Vertical Plates, ASME Journal of Heat Transfer, vol. 113, pp. 620–626, 1991.
- [32] Batchelor, G. K., An Introduction to Fluid Dynamics, Cambridge University Press, Cambridge, UK, 1967.
- [33] Zwart, P. J., Raithby, G. D., and Raw, M. J., An Integrated Space— Time Finite-Volume Method for Moving-Boundary Problems, *Numerical Heat Transfer B*, vol. 34, pp. 257–270, 1998.
- [34] Gaskell, P. H., and Lau, A. K. C., Curvature Compensated Convective Transport: SMART, a New Boundedness Preserving Transport Algorithm, *International Journal of Numerical Methods for Fluids*, vol. 8, pp. 617–641, 1988.
- [35] Darwish, M., and Moukalled, F., Normalized Variable and Space Formulation Methodology for High-Resolution Schemes, *Numerical Heat Transfer B*, vol. 26, pp. 79–96, 1994.
- [36] Patankar, S. V., Numerical Heat Transfer and Fluid Flow, Hemisphere Publishing Corporation, New York, 1980.
- [37] Moukalled, F., and Darwish, M., Pressure Based Algorithms for Single and Multifluid Flow, in *Handbook of Numerical*

- *Heat Transfer*, 2nd edition, W. J. Minkowycz, E. M. Sparrow, and J. Y. Murthy (eds.), pp. 325–367, Wiley, New York, 2006.
- [38] Moukalled, F., and Darwish, M., A Unified Formulation of the Segregated Class of Algorithms for Fluid Flow at All Speeds, *Numerical Heat Transfer B*, vol. 37, no. 1, pp. 103–139, 2000.
- [39] Peric, M., A Finite Volume Method for the Prediction of Three Dimensional Fluid Flow in Complex Ducts, Ph.D. Thesis, Imperial College, Mechanical Engineering Department, London, UK, 1985.



Fadl Moukalled is a professor of mechanical engineering at the American University of Beirut. He received his Ph.D. in 1987 from Louisiana State University. His research interests include computational fluid dynamics, numerical heat transfer, and finite-time thermodynamics. His current research is geared toward numerically predicting supersonic mixing and evaporation of liquid droplets in a stream of air following a pressure-based MUSIG /H-MUSIG approach.



Issam Lakkis is an assistant professor of mechanical engineering at the American University of Beirut. He received his Ph.D. in 2000 from MIT (Cambridge, MA). His research interests include CFD development and applications (mainly vortex methods for reacting flows) and MEMS simulation and modeling.